SLAC-P
Decembe
(A)

SLAC-PUB--5717

DE92 006431

SLC BEAM DYNAMICS ISSUES*

John T. Seeman
Stanford Linear Accelerator Center, Stanford University, Stanford, California, 94309

Abstract

The Stanford Linear Collider (SLC)[1,2] accelerates single bunches of electrons and positrons to 47 GeV per beam and collides them with small beam sizes and at high currents. The beam emittances and intensities required for present operation have significantly extended traditional beam quality limits. The electron source produces over 10^{11} e^- in each of two bunches. The damping rings provide coupled invariant emittances of 1.8×10^{-5} r-m at 4.5×10^{10} particles. The 50 GeV linac has successfully accelerated over 3×10^{10} particles with design invariant emittances of 3×10^{-5} r-m. The collider arcs are now sufficiently decoupled and matched in betatron space, so that the final focus can be chromatically corrected, routinely producing spot sizes (σ_x, σ_y) of 2.5 μm at the interaction point. Spot sizes below 2 μm have been made during tests. Instrumentation and feedback systems are well advanced, providing continuous beam monitoring and considerable pulse-by-pulse control. The luminosity reliability is about 60%. Overviews of the recent accelerator physics achievements used to obtain these parameters and the present limiting phenomena are described for each accelerator subsystem.

1.0 Introduction

The present operating parameters of the SLC during colliding beams for high energy physics are shown in Table 1. The best parameters in each category obtained during tests are also shown (not taken under simultaneous conditions). The goals for 1992 with the SLD physics detector are shown to indicate which parameters are under active improvement[3].

2.0 Electron source

The recent main task for the electron injector has been to develop a method to transport high charge, multiple electron bunches from the gun and buncher to the damping ring while maintaining reasonable emittances, good energy spreads, and equal energies[4].

The stability of the injector has been significantly improved through reproducible accelerator parameter configurations developed to maintain high current levels. These configurations often remain appropriate for weeks.

The emittance of the high charge electron beam at the entrance to the damping ring has often been too large, causing particle loss and enhanced emittance on extraction. This enlarged emittance has been traced to transverse wakefields in the early accelerating structure in the injector (30 to 200 MeV). An addition of a betatron oscillation to the beam at the appropriate phase over the later two thirds of the injector (80 m) produces additional wakefield effects which cancel the earlier wakefield effects[5]. More information on these cancelling oscillations is given in Section 5. With these corrections 5.6×10^{10} e^- in one bunch and 4.7×10^{10} e^- in each of two bunches (4×10^{10} is routine) have been extracted from the e^- ring. Loading and transverse wakefields in the subharmonic buncher and s-band structure make the two bunches have different trajectories and RF phases and, thus, impact their respective intensities.

The positron system, after extensive tuning, achieved a yield of 1.25, meaning the ratio of the number of positrons captured in the damping ring to the number of incident 30 GeV electrons on the conversion target[6]. The main gains came from aligning the injector linac (90 m), beta matching the positrons into the linac, and fixing aperture restrictions just upstream of the damping ring. A positron charge of 3.8×10^{10} in a single bunch has been injected into the main linac.

* Work supported by Department of Energy contract DE-AC03-76SF00515.

Invited talk at the 5th ICFA Advanced Beam Dynamics Workshop on "Effects of Errors in Accelerators, Their Diagnosis and Correction," Corpus Christi, TX, October 3-8, 1991.

Table 1 1991 SLC Accelerator Parameters

Accelerator Parameter	Units	1984 Design	Best Indepen-dently Achieved	Simultaneous during 1991 SLD Collisions	Goal for 1992 SLD Collisions
Beam energy	GeV	50	53	46.6	46.6
Repetition rate	Hz	180	120	60	120
Energy spectrum	%	0.25	0.2	0.3	0.3
N^- at IP	10^{10}	7.2	3.5	2.8	>3.5
N^+ at IP	10^{10}	7.2	3.2	3.0	>3.5
N^- in Linac	10^{10}	7.2	4.6	3.1	4.0
N^+ in Linac	10^{10}	7.2	3.8	3.3	4.0
N^- (210 MeV)	10^{10}	8.0	7.0	5.0	8.0
N^+ (210 MeV)	10^{10}	14.0	10.0	9.0	10.0
e^+ yield	e^+ / e^-	1.0	1.25	1.0	1.1
$\gamma\varepsilon^+_{x(y)}$ in Linac	10^{-5} r-m	3.0 (3.0)	2.0 (2.0)	2.7 (2.7)	3.0 (3.0)
$\gamma\varepsilon^-_{x(y)}$ in Linac	10^{-5} r-m	3.0 (3.0)	2.1 (2.0)	3.0 (2.8)	3.0 (3.0)
IP beam divergence	μrad	300	300	290	300
IP beam size in x	μm	2.07	<2.0	2.5	<2.0
IP beam size in y	μm	1.65	<2.0	2.5	<2.0
Bunch length (σ_z)	mm	0.5-1.5	0.5-12.	1.1	1.2
Pinch enhancement		2.2	1.0	1.0	1.1
Luminosity	$10^{30}/cm^2sec$	6.0	0.077	0.077	0.5
Efficiency (Accel)	%	100	90	50	50
Polarization	%	39	0	0	34

3.0 Damping ring

The primary activities in the damping rings have been to achieve small beam emittances at high bunch charges. Two phenomena stand out: 1) a longitudinal π mode instability develops above about 3×10^{10} particles per bunch and 2) the horizontal emittance does not damp properly for the first one half damping time.

The longitudinal π mode instability[7] causes unwanted random trajectory changes upon extraction where there is finite dispersion and leads to unwanted emittance growth. The instability depends upon the RF cavity temperature and tuner positions. At high currents the π mode instability is very sensitive to these parameters and is difficult to control. An idling feedback cavity is under construction to reduce this unwanted effect. Longitudinal feedback for the π mode has been tried using signals from the two bunches separately[8]. The initial results are promising but further work is needed.

At long storage times (1/60 second) the extracted emittances were measured to be equal to the design equilibrium values. However, at shorter times (namely 1/120 second needed for 120 Hz operation) the electron horizontal emittance had not damped sufficiently[9]. Further study of the emittance versus storage time showed that the horizontal emittance did not damp properly over the first few milliseconds, but damped properly thereafter. This effect can be seen in Figure 1. With an uncoupled ring the vertical emittance damping appeared to be correct. At early times, the horizontal beam had a significant non-gaussian horizontal distribution, which became gaussian at about 5.5 msec. Effects of launch parameters (x, x', E, σ_E/E), synchro-betatron coupling[10], or tune dependent amplitudes do not appear to be the cause. The only parameter which has been shown to affect the damping is the horizontal tune, but with an unexpected slowly varying manner as is shown in Figure 2. A new operating point with a horizontal tune of 8.25, increased from the nominal 8.17, will be tried during the next run.

The full coupling of the beams in the damping ring is important for maintaining round beams at the interaction point. The natural coupling resonance in the damping ring is quite small and small tune variations in the ring from trajectory drifts caused the beam to come out of coupling often. Now, vertical closed bumps through sextupoles are added to the beam trajectory to broaden the coupling resonance.

4.0 Bunch length compressor

In the transport line between the damping ring and the linac, the bunch length is shortened from 6-9 mm to 1 mm. This shortening is done by introducing a head-tail energy difference and having a non-isochronous bend. Many emittance enlargement effects may occur in this region from betatron mismatches, dispersion mismatches, x-y coupling, static injection offsets, and launch jitter. The large dispersion and the large energy spread required for length compression are serious complications.

Betatron mismatches occur when the injected beam has a phase-space orientation (β,α) that does not match the linac lattice. Because of geometry the linac lattice cannot be chromatically corrected.

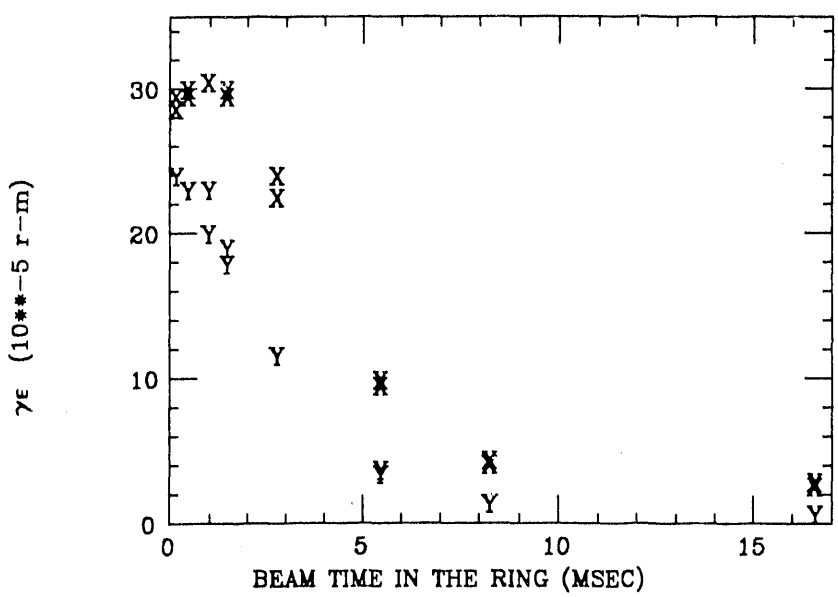

Figure 1 Measured extracted beam emittances versus storage time in the damping ring.

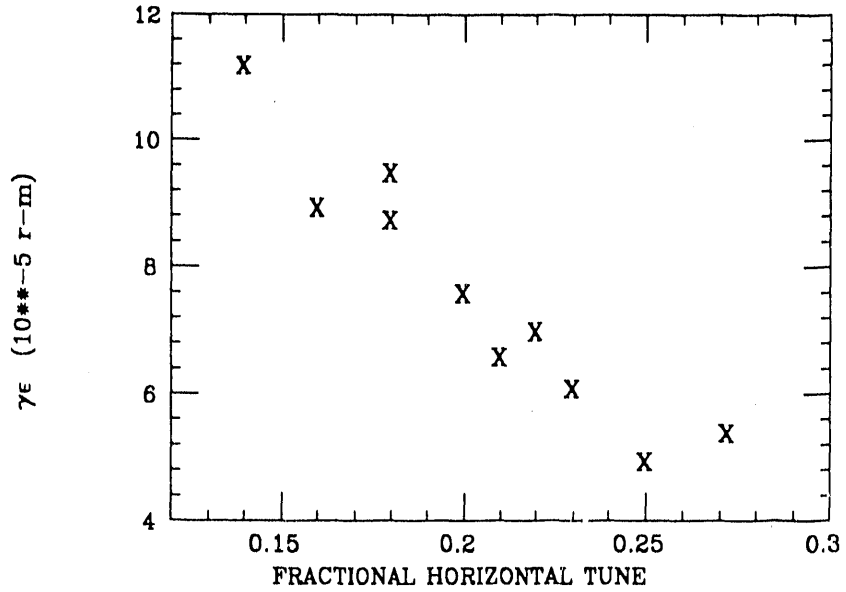

Figure 2 Measured extracted horizontal beam emittance at 5.6 msec versus damping ring horizontal tune.

Therefore, particles with different energies have different oscillation frequencies. Since the injected beam has an internal energy spread that changes during acceleration, the trajectories of the different energy portions of the beam rotate in phase space at different speeds and soon undergo filamentation. Given a beam β_b and α_b that are mismatched from the lattice design values β_l and α_l, the emittance enlargement after filamentation is given by a parameter Bmag[11].

$$(\gamma\varepsilon)_{final} = \text{Bmag}\,(\gamma\varepsilon)_{initial} \tag{1}$$

with

$$\text{Bmag} = \frac{1}{2}\left[\frac{\beta_l}{\beta_b} + \frac{\beta_b}{\beta_l} + \beta_b\,\beta_l\left(\frac{\alpha_b}{\beta_b} - \frac{\alpha_l}{\beta_l}\right)^2\right] \tag{2}$$

To avoid emittance increases of order 10%, β_b must be matched to about 30%. The α_b match has a similar constraint. The measured beam size at the end of the linac as a function of a quadrupole strength error early in the linac is shown in Figure 3.

Dispersion mismatches are similar[12,13]. A dispersion η is a transverse position-energy correlation which adds to the apparent size and emittance of the beam: $\sigma^2 = \varepsilon\,\beta + \eta^2\,(\delta)^2$. The measured effective emittance ε_{eff} in the presence of dispersion[11] is given by

$$\varepsilon_{eff}^2 = \varepsilon_\beta^2 + \frac{\varepsilon_\beta}{\beta_l}\left[\eta^2 + \left(\beta_l\,\eta' + \alpha_l\,\eta\right)^2\right]\left\langle\delta^2\right\rangle \tag{3}$$

Given the chromatic linac lattice, the particles displaced by dispersion undergo filamentation if allowed and the real emittance grows. With filamentation the emittance increases further leading to a final value of

$$\varepsilon_{eff} = \varepsilon_\beta + \frac{1}{2\,\beta_l}\left[\eta^2 + \left(\beta_l\,\eta' + \alpha_l\,\eta\right)^2\right]\left\langle\delta^2\right\rangle. \tag{4}$$

The errors in the dispersion at injection must usually be controlled to a few millimeters. Minimization of the measured emittance early in the linac is done by adjusting quadrupoles in a dispersive region upstream to remove the final dispersion errors. Examples of the minimization of emittance using dispersion controls are shown in Figure 4.

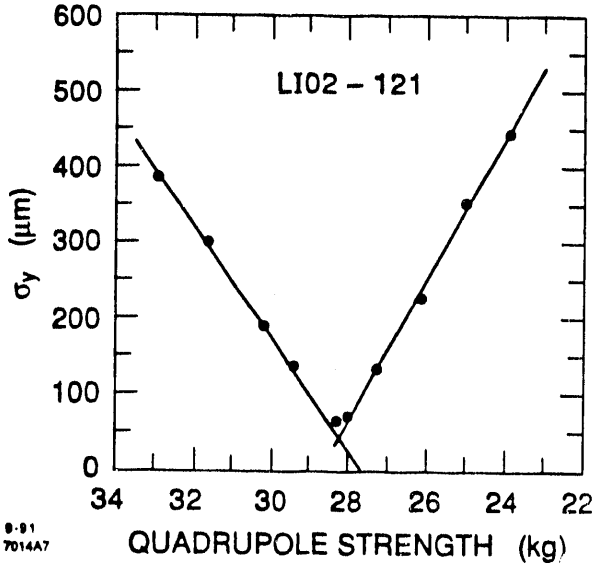

Figure 3 Measured beam size at the end of the linac versus the strength of an early quadrupole.

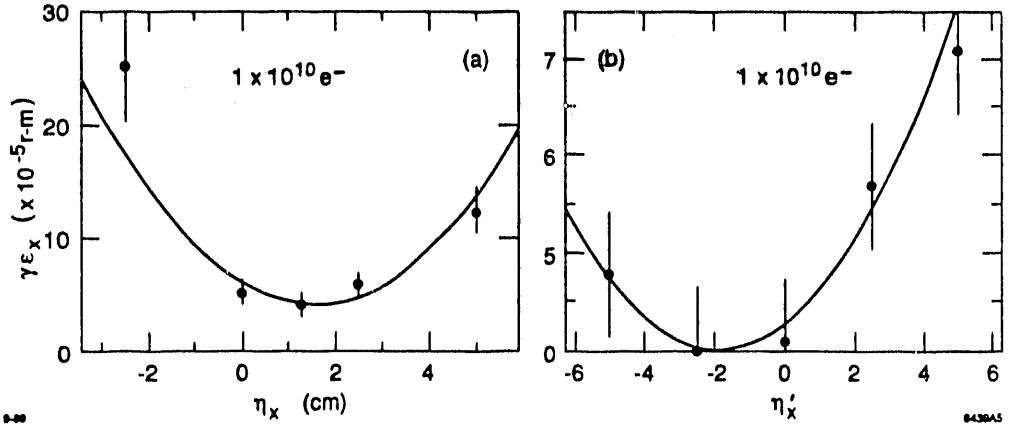

Figure 4 Measured emittances at the end of the SLC accelerator as a function of dispersion errors at injection. The solid lines are theoretical predictions.

The large energy spread in the beam ($\sigma_E/E = 1\%$) allows errors in the second order transport to affect the emittance and betatron match. The introduction of independent sextupole power supplies has provided a nearly complete set of second-order orthogonal dispersive and betatron chromaticity adjustments, which have successfully corrected most of the desired terms[14]. Still remaining, however, is a 30% increase in emittance from still higher order terms driven by the energy spread.

The higher order fields contribute to transport considerations. Because the beam in the transport line at several points fills the horizontal vacuum chamber (6.5 cm), dipole and quadrupole fringe and pole tip fields must be carefully controlled during manufacturing or compensated later with great care. An example of the effects of second- and third-order fields is shown in Figure 5 where the beam emittance at the entrance to the linac contains higher order terms in the energy spread[15]. Two octupole magnets are being installed for correction of this effect. To indicate the magnitude of the correction required for the 1.15 GeV beam, each octupole is 10 cm long with a bore of 6.5 cm and has a pole tip field of 40 gauss.

Since the beam aspect ratio in this transport line is as large as 250, small skew quadrupoles are needed to compensate for quadrupole rotation errors. Two magnets make a complete set, but a single magnet has been shown to be adequate.

The emittances of the beam at injection into the linac are important as they give the scale of the tolerances to be studied downstream. The measured emittances at the entrance to the SLC linac are shown in Figure 6 including the improvements discussed above[16]. The horizontal emittance increases with intensity because of bunch lengthening with current in the damping ring[17] leading to larger energy spreads during compression and effects from higher order fields that are not yet compensated.

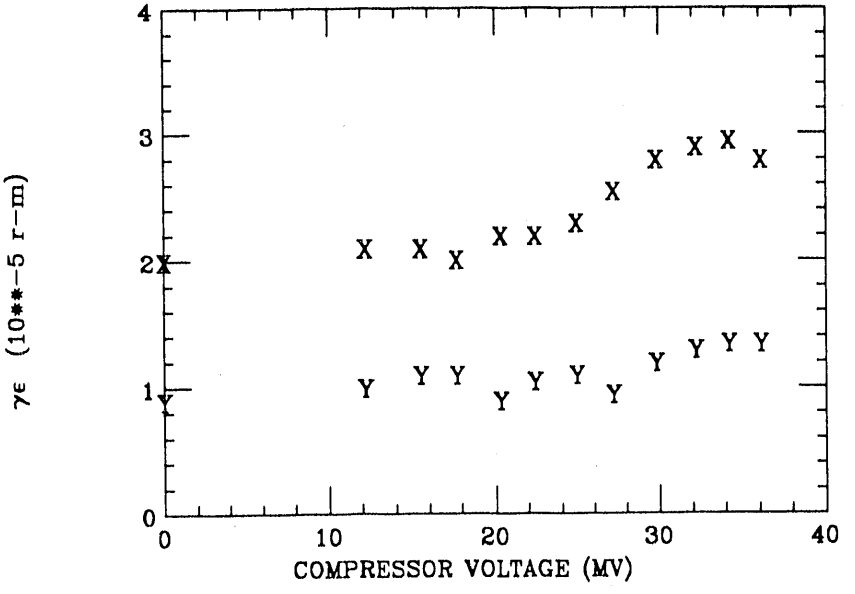

Figure 5 Measured emittance at the entrance to the linac versus the RF voltage on the bunch length compressor in the ring-to-linac transport line.

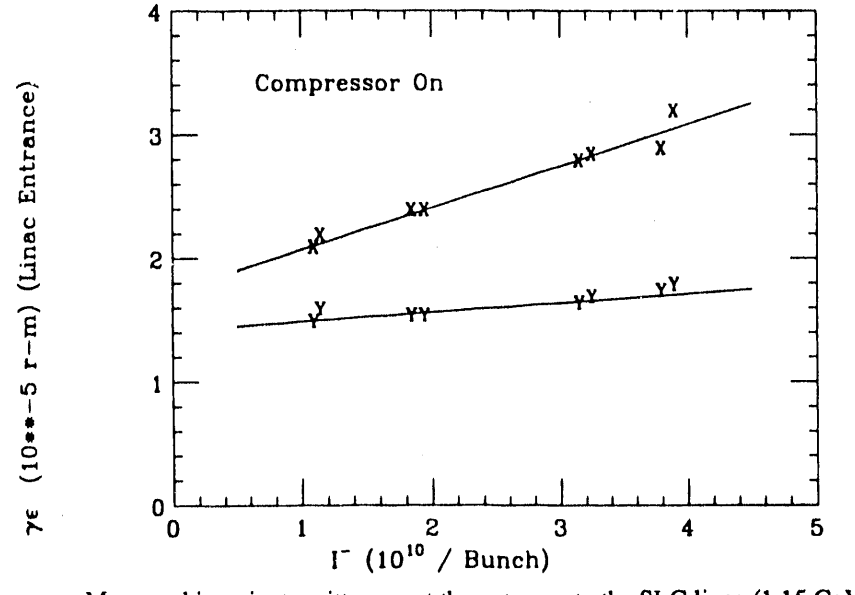

Figure 6 Measured invariant emittances at the entrance to the SLC linac (1.15 GeV) as a function of the beam intensity with the bunch length compressor excited in the standard configuration. The vertical emittance remains constant but the horizontal emittance grows. This growth is associated with first- and second-order chromatic errors in the transport line (σ_E/E= 1%) and the onset of bunch lengthening in the damping ring at about 1 x 10^{10} e^-.

5.0 Linear accelerator

Acceleration in the linac damps the absolute emittance by the square root of the ratio of the initial to final energies which is a factor of 41 for the SLC. The primary goal for linac operation is to prevent any additional effects from increasing the emittance. There are many possible enlargement effects[18]. However, injection oscillations and errors in steering and alignment are especially important at present. A summary of wakefield studies and cures is given in Reference 19.

A static launch error of the beam injected into the linac generates a betatron oscillation. Standard trajectory correction restores the proper launch. There are several position-angle feedback systems distributed along the accelerator to keep the trajectory stable. These have worked exceptionally well and have mostly released the accelerator operators from the task of constant trajectory control.

However, if the launch of the beam fluctuates more rapidly than feedback can correct it, other methods of control are needed. The transport equation of motion for particles in the bunch can be used to study oscillations along the linac.

$$\frac{d^2}{ds^2} x(z,s) + k^2(z,s)\, x(z,s) = \frac{r_e}{\gamma(z,s)} \int_z^{\infty} dz'\, \rho(z') W_r(z'-z)\, x(z',s), \qquad (5)$$

where s is the distance along the accelerator; z is the distance internally along the bunch; k is the quadrupole focusing term (which varies along the linac and along the bunch because of energy changes); ρ is the line density; W_r is the transverse wakefield due to the accelerating structure; and r_e is the classical electron radius. The left-hand side of Equation 5 represents the form of a betatron oscillation including (slow) acceleration. The right-hand side indicates the forces from transverse wakefields on each particle generated by position errors in the accelerating structure of all the preceding particles in the bunch. The transverse wakefields for the SLC structure increase in strength with the distance between the leading and the trailing particles[20]. Thus, the particles at the back of the bunch, in general, see the largest forces. The displacements grow exponentially with distance along the linac[19]. This strongly forced oscillation of the tail by the head (seen in Equation 5) can be ameliorated by changing the energy spectrum along the bunch so that the head is higher in energy than the tail; this can be accomplished with RF phasing adjustments. The wakefield forces, which act like a defocusing force on the tail of the bunch, can be mostly cancelled by the increased focusing of the tail by the quadrupole lattice. This effect is called BNS damping[21]. BNS damping has been studied at the SLC[22] and has been shown to be so effective that all SLC linac operations now use it. The BNS settings used for SLC operations at 3×10^{10} particles have the first 56 klystrons phased at -20 degrees and the remaining klystrons phased at +15 degrees. In all cases the overall linac phase is adjusted to make the energy spectrum small (about 0.3%) at the end of the accelerator.

The cancellation of wakefield forces by BNS damping may be exploited further. By careful arrangement of the bunch charge density based on knowledge of the local beam energy, lattice, bunch length, and RF structure, nearly all particles in the bunch can be made to follow exactly the same trajectory. The conditions for this behavior can be derived by substituting an identical oscillation into Equation 5 for all particles, and cancelling position terms on both sides[23]. This condition is called autophasing[24]. However, simulations and experimental attempts to match this special condition in the actual operation of the SLC have not been fruitful to date, though studies continue.

Misalignments of quadrupoles, position monitors, and accelerating structures in the linac cause each beam (after correction) to have a trajectory that is neither straight nor centered in the accelerating structure. These offsets generate dispersion and wakefield emittance growth as described above. There are several methods to deal with these errors. (a) They can be found mechanically and fixed, although the required accuracy is well below 100 mm[25]. (b) Calculations using knowledge of the beam trajectory as a function of the quadrupole lattice strength can determine the relative quadrupole and position monitor errors to about 75 to 100 mm[26]. The misalignments can then be mechanically corrected. (c) A dispersion reducing trajectory correction may be tried[27]. (d) Mechanical movers of the RF structure in the tunnel can be used in a betatron harmonic correction scheme to reduce the final emittance[28]. (e) Betatron oscillations can be forced onto the beam at various locations along the linac

to cancel effects of the existing absolute trajectory and thus minimize the final emittance[29]. (f) Finally, harmonic changes can be added to the quadrupole lattice to cancel random and systematic errors in the quadrupole field strengths[30]. The best combination of the available solutions depends on the particular errors involved. All have been tried on the SLC linac with various degrees of success[16].

Mechanical vibration of quadrupoles in the SLC can potentially cause trajectory jitter in the beams, resulting in dispersion and wakefield emittance growth. Studies in the SLAC tunnel of the linac quadrupoles and their supports show vibrations at the 0.05-μm level, mostly with frequencies below 10 Hz. Quadrupoles centered on long girders (12 m) show 0.5-μm vibration levels at the resonant frequency of the girder (about 8 Hz). These levels are adequate for the SLC but study is needed for the next collider.

After the input parameters are optimized and the trajectory nominally corrected, the beam experiences emittance growth during acceleration because of align nent errors of the accelerator components. This results from the trajectory being steered through misaligned quadrupoles and accelerator structures onto beam position monitors with finite residual offset errors. Consequently, transverse wakefields excite the beam. Methods to reduce these effects have been theoretically studied[31,32]. It has been shown that the addition of appropriate injection errors (Δx, $\Delta x'$, Δy, and $\Delta y'$) can cancel most of the emittance enlargement. Since the advent of BNS damping, a more global scheme of distributing short range oscillations along the accelerator has been shown to be satisfactory[33]. Oscillations have been added to the SLC linac to test this procedure. Examples of these oscillations are shown in Figure 6. The emittance at full energy was measured as a function of the oscillation amplitude. The results are shown in Figures 8 and 9. A proper choice of the amplitude of a short range oscillation in the appropriate linac location can significantly reduce the emittance enlargement. Furthermore, the betatron match of the beam can be left properly maintained. Combinations of short range (200 m) oscillations in the SLC were applied to the two beams during particle physics collisions, and the emittances were reduced to the design values at 3×10^{10} e^-. The required electron trajectories for reducing the emittances during the August 1991 run are shown in Figure 10. Note that significant trajectory offsets were needed for this optimized case.

At high currents the alignment of the RF structure relative to the quadrupoles and position monitors dominates all other alignment issues. Great efforts have been made to develop techniques which can align the structures to these tolerances and to keep them aligned over a long period with minimal effort. Experiments have taken place to study wakefields in misaligned structures[34]. Experimentally, it has been shown that moving structure irises with no other changes can deflect the beam[19]. The component of the structure alignment errors at the betatron spatial frequency is primarily that which drives the beam. Therefore, if a control mechanism can be made to move the structure at that spatial frequency, then sine and cosine adjustments can be used to cancel the accumulation of alignment errors over reasonably short regions of the accelerator[35]. This control can also be used to correct for any long term position drifts of the accelerator or quadrupole supports due to temperature changes or floor creep in the tunnel. A 100 m test of this active control is underway in the SLC Linac.

Operations and studies of the SLC have shown that these emittance enlargements from chromatic and wakefields effects can be controlled during colliding beam operations to provide significant luminosity[16]. The best measured single bunch emittance conditions of the SLC to date are shown in Figure 11. These results were also obtained during collisions with three bunch operation (e+,e-, e- scavenger) up to 3×10^{10} particles per bunch. An extension of these techniques to higher currents is now under active study as intensities near 4.5×10^{10} are needed and the excessive horizontal beam jitter at high currents mentioned in the next section must be reduced.

6.0 Injection jitter

Feedback systems that work pulse-by-pulse are essential for keeping the beam parameters within acceptable limits given the many possible sources of transverse jitter: varying power supplies of dipoles and off axis quadrupoles, vibrating quadrupoles, klystron phase and amplitude jitter, unstable kicker magnets, and changes in the beam intensity. In the SLC, over 80 beam parameters (beam positions, angles, and energies) are controlled by feedback routinely with many corrections each second. Not all parameters need rapid feedback. For example, the energy spectrum feedback has proven not to need pulse-by-pulse control. Modern control theory is used to provide cascaded control of position and angle loops from the beginning to the end of the accelerator that minimally interfere with each other

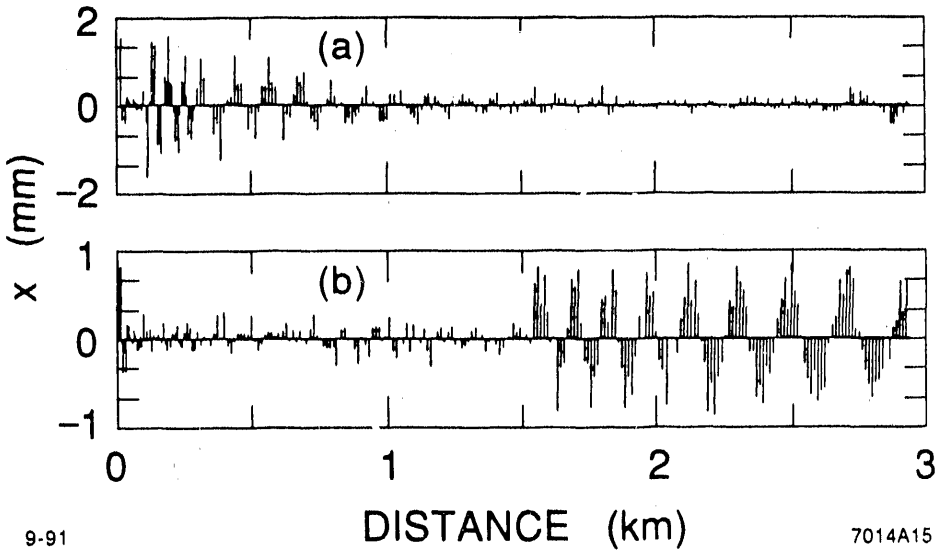

Figure 7 Two induced oscillations in the SLC accelerator used to cancel accumulated wakefields and dispersion errors in the linac, see Figures 8 and 9.

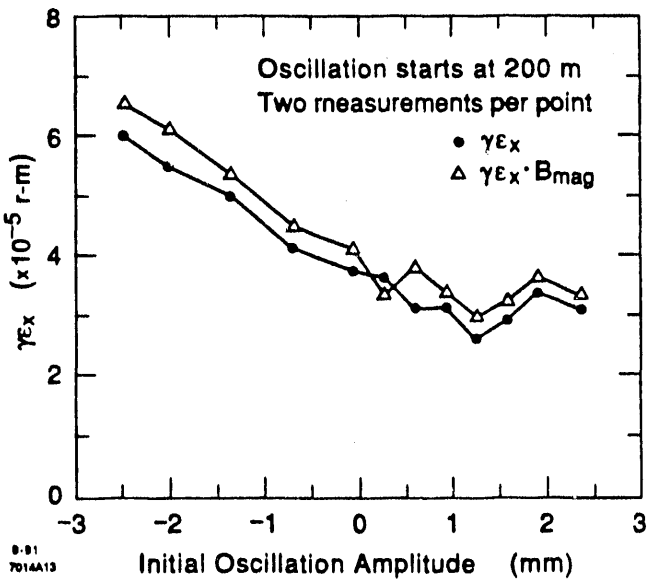

Figure 8 Invariant emittance changes at the end of the linac (47 GeV) as a function of the amplitude of an oscillation starting early in the linac (upper plot in Figure 7). The emittance measurements and the emittance times Bmag measurements track each other very well. Since Bmag is a measure of the expected filamentation from betatron mismatches, the beam at the end of the linac has already filamented. A decrease in the transverse emittance (25%) is observed with a finite oscillation added to the beam. The error which caused the original emittance enlargement is thus near the beginning of the linac.

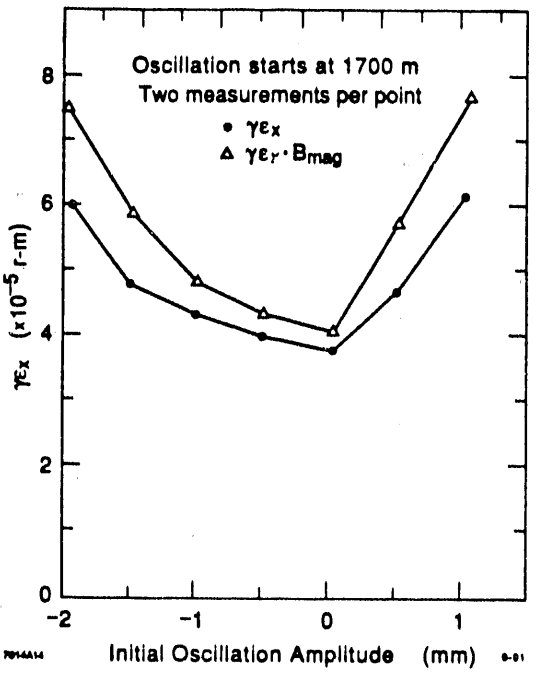

Figure 9 Invariant emittance changes at the end of the linac (47 GeV) as a function of the amplitude of an oscillation starting in the center of the linac (lower plot in Figure 6). There is no reduction of the emittance from this oscillation and, furthermore, a large betatron mismatch has developed signaled by the separation of the curves for γε and γε x Bmag.

and provide maximum control[36]. Reduction of oscillations with frequencies up to one sixth of the accelerator pulse rate can be expected.

Injection jitter too rapid for feedback control must be isolated and fixed. The sources of jitter are generally not stable, and, thus, sophisticated analysis techniques must be developed. The magnitude of the jitter can depend strongly on current. An observation in the SLC is shown in Figure 12 where the horizontal jitter becomes rapidly stronger above 3.5 x 10^{10} e^- per pulse[37]. The nature of this jitter can be seen in Figure 13. The signature of the oscillations does not resemble that of a nominal betatron oscillation generated by a single dipole. A quadratic departure from the axis along the bunch closely matches the data[38]. The probable cause for this rapid change is the combination of the large dispersion in the transport line between the damping ring and the linac and the lengthened bunch in the damping ring at high currents. In addition, small bunch length or quadrupole mode oscillations in ring are present as well as small RF phase oscillations (0.2^0) of the bunch. The particles at the front and back of the bunch are at large amplitudes in the transport line and are focused incorrectly because of high order fields. Given the asymmetries of the high order fields and the collimation of off-energy particles by the apertures and phase jitter, these particles probably enter the linac far off axis and far ahead or behind the main core of the beam. The head particles then excite wakefields downstream.

If a bunch has a skew profile as it enters the accelerator, it is not possible to correct the bunch with steering to remove all transverse wakefield effects downstream. Dispersion at the entrance to the accelerator can cause a partially compressed bunch to have a transverse-longitudinal tilt. $\Delta x = \eta\, \Delta E/E$. The head of the bunch is not on axis even though the average position of the bunch is. The oscillation of the head downstream will likely drive the trailing portions of the bunch to large amplitudes, increasing the emittance. Calculations of this effect for the SLC linac give a tolerance on the allowed dispersion as a function of current[39]. The results are shown in Figure 14. Besides the removal of the dispersion errors, careful placement of the bunch and the use of BNS damping are quite helpful. However, jitter in the energy of the beam entering the linac can make this problem especially troublesome. Thus, the dispersion is controlled to a few millimeters at the entrance of the SLC linac.

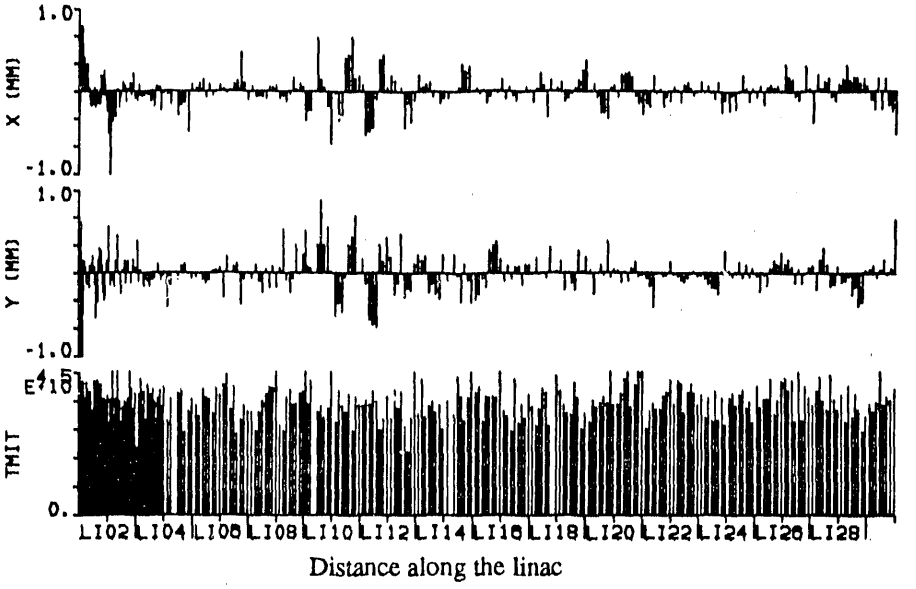

Figure 10 Empirically determined linac trajectory which cancels the errors from the accumulation of dispersion and transverse wakefields errors at 3 X 10^{10} e^-. This oscillation lowered the horizontal emittance from 4.5 to 3.0 (X 10^{-5} r-m). This trajectory is not unique as other trajectories with similar oscillations can produce the same effect. This non-zero trajectory remained the optimum trajectory during several weeks of collisions.

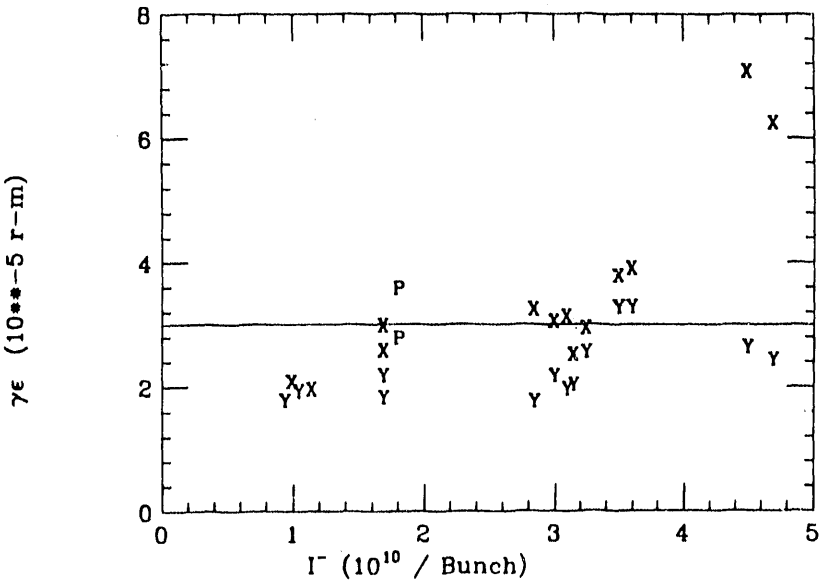

Figure 11 Best measured invariant emittances at the exit of the SLC linac (47 GeV) as a function of beam current. The symbol P refers to positrons. Emittances (x and y) at 1 X 10^{10} electrons have been measured at 2 x 10^{-5} r-m, which is 67% of the desired value of 3 x 10^{-5} r-m. At 3 x 10^{10} electrons the design emittance values were obtained. Above about 4.0 x 10^{10} e^-, a strong launch jitter is produced from the damping ring system and amplified in the linac which causes larger emittances. Comparing with Figure 6, a sizable fraction of the emittance growth up to 3 x 10^{10} e^- is caused by the increase in the injected emittance.

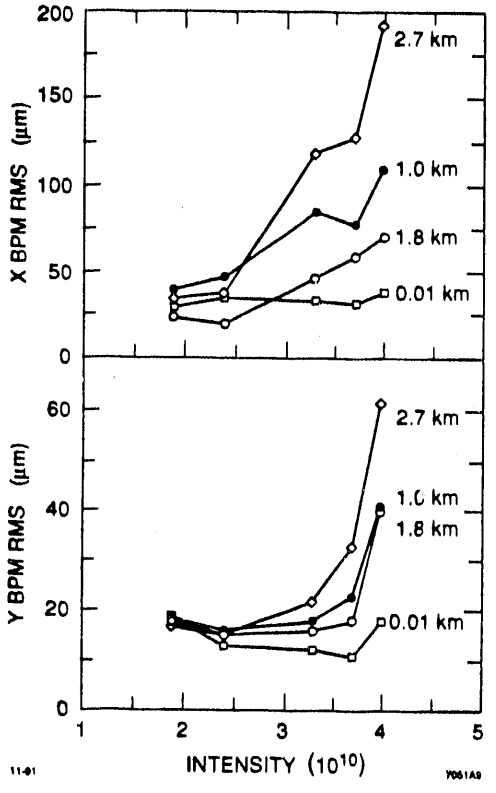

Figure 12 Measured transverse position jitter in the SLC e^- beam as a function of current and position along the linac. At low currents, all positions have similar rms jitter values. However, at high currents the locations downstream indicate much stronger oscillations. Other observations suggest that the injected beam has a longitudinal quadratic offset profile which causes increased jitter effects in the linac, see Figure 13.

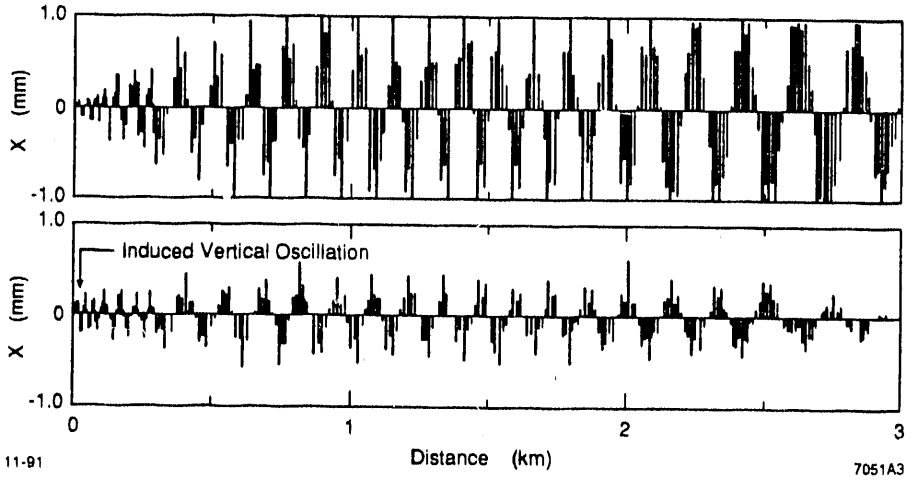

Figure 13 A horizontal oscillation resulting from the unknown jitter source shown in Figure 12 at 4 x 10^{10} e^- in the SLC. A vertical oscillation was also produced but with a deliberate change in a dipole magnet early in the linac. The vertical oscillation is not the same as the horizontal, indicating that the transverse offsets over the length of the bunch are not like those from a dipole deflection but more likely a higher moment.

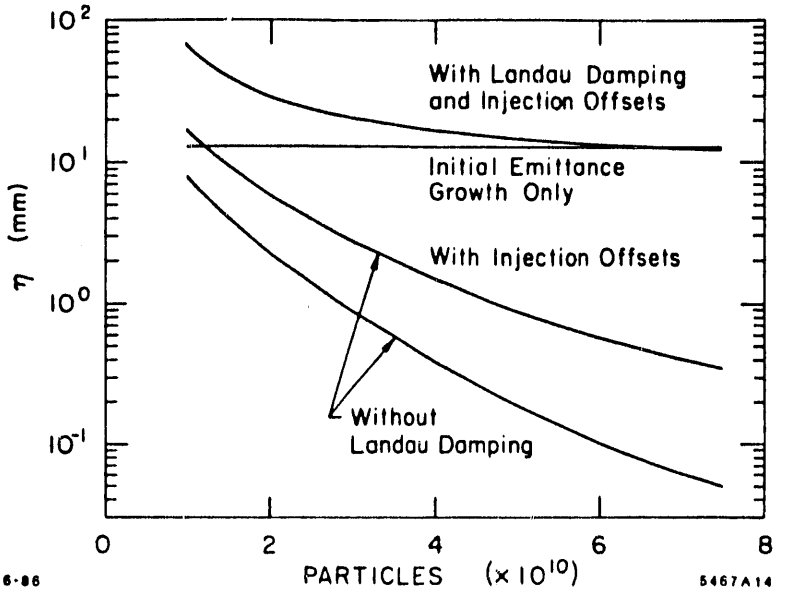

Figure 14 Upper limits on the allowed residual dispersion η entering the SLC linac as a function of bunch intensity. The limits are calculated for a partially compressed bunch (1.5 mm) where dispersion tilts the bunch transversely and excites transverse wakefields in the linac. Steering the head of the bunch near the axis of the accelerator increases the tolerances. Also, BNS damping (Landau) increases the tolerances significantly. Higher order dispersion will have equivalent effects.

7.0 Arcs

The arcs must transport two high energy bunches from the linac to the final focus without significant emittance dilution[40]. The arc system is comprised of a short matching region at the end of the linac leading into a very strong focusing FODO array of combined function magnets including dipole, quadrupole, and sextupole fields. Each lattice cell has a betatron phase advance of 108 degrees and a length of 5 m. Each 47 GeV particle loses about 1 GeV to synchrotron radiation in a single pass through the system. Ten pairs of magnets form a second order achromat that can safely transport beams with an energy spectrum of 0.5%. There are 23 [22] achromats in the north [south] arc. At the end of each F [D] magnet within an achromat a beam position monitor is attached to sense the x [y] beam position with an accuracy of about 25 μm. The combined function magnets are moved by motorized jacks for beam steering.

Achromat units (20 magnets) as groups were rotated around the beam axis up to 10 degrees to provide the needed vertical bending for terrain following. Initial matching problems and slight phase advance errors over the length of an achromat cause unwanted coupling of vertical and horizontal beam motion at the roll boundaries. Also, magnet misalignments contribute to unwanted emittance enlargements. A combination of several solutions has now produced acceptable results: tapered rolls at the achromat boundaries, betatron phase corrections using backleg coils on the magnets, trajectory steering by magnet movers, harmonic corrections at certain spatial frequencies, and 3π trajectory bumps for skew correction are all distributed where needed along the arcs[41]. These corrections are made after exhaustive oscillation data are taken throughout the arcs starting in the linac. After measuring the actual first-order transport matrix R_{ij}, one can implement the appropriate corrections[42].

Time dependent variations of the dispersion entering the final focus were traced to day-night thermal fluctuations in the cooling water temperature of the early arc magnets. This effect resulted in quadrupole and arc magnet displacements which primarily changed the dispersion function. Improvements in the temperature regulation and tuning adjustments will ameliorate this problem.

Finally, a recent discovery that a betatron mismatch entering the arcs can increase the emittance growth due to synchrotron radiation has forced a better betatron match[43]. An improvement in the horizontal emittance growth due to radiation in the arcs by a factor 2 (from 2×10^{-5} r-m to 1×10^{-5} r-m) was obtained with moderate quadrupole adjustments.

8.0 Final Focus

The final focus system of the SLC must focus the two opposing beams to small sizes at the collision point and it must steer the two beams into head on collision. To a large extent, recent efforts have been spent on tuning algorithms for small spots and alignment of the final focus triplets.

In the final focus, the beam first enters a correction region to remove dispersion entering from upstream. Then the beam passes through the first demagnifying telescope where the x and y planes have demagnifications of 8.5 and 3.1, respectively. Betatron mismatches and x-y coupling arriving from upstream are also corrected in this region. Next, the chromatic correction section, which contains gentle bends and sextupoles, is used to correct the trajectories of different energy particles so that they focus at the same longitudinal position at the interaction point (IP). The final telescope provides the last demagnification to make the smallest spots possible and to make the vertical and horizontal spots have equal size. After passing through the IP, each beam traverses through the opposing beam's transport line and is deflected into an extraction line to a high power dump. New superconducting quadrupoles have been installed with the SLD detector. These quadrupoles are closer to the IP. They allow a reduced β^* and a doubling of the potential luminosity[3].

The minimum spot sizes at the IP depend on the incoming beam emittances, the maximum allowed divergence angles at the IP, and chromatic corrections. The design values for the incoming beam emittances ($\gamma\varepsilon$) are 4.5×10^{-5} r-m horizontally and 3.5×10^{-5} r-m vertically. However, during current operation the actual emittances are about 35% higher. The angular divergence is limited by synchrotron radiation coming from the strong focusing quadrupoles near the IP. The masking near the detector limits the angular divergence to 300 μrad for the SLD. Finally, the chromatic corrections[44] are made by eliminating the unwanted first-, second-, and third-order matrix elements: R_{ij}, T_{ijk}, U_{ijkl}, respectively.

The beams are very dense at the collision point and can exert large transverse forces on each other, referred to as beam-beam deflections. As the two beams are steered through each other, the beam-beam deflection first adds and then subtracts from the bending angle. An example[45] of a measured beam-beam deflection is shown in Figure 15. Beam-beam deflections can be measured in the horizontal, vertical, and skew planes. From the observed deflections, many beam properties can be derived. The beam centroid offsets are determined from the place where the deflection crosses zero. This offset is removed by using nearby dipole magnets to bring the beams into head on collision. The shape of the deflection curve indicates the size of the combined two-beam system and is a good indicator when upstream components have changed the beam parameters. Jitter in the deflection measurements often indicates pulse-by-pulse position changes. Present jitter is about one third of the beam size as can be seen in Figure 16 and results in only a small loss in average luminosity. A pulse-by-pulse feedback system keeps the beam in collision using these signals.

The particles bent in the beam-beam interaction radiate a form of synchrotron radiation called "beamstrahlung". This radiation travels forward and is detected using a gas Cerenkov detector about 40 m downstream. The radiation from one beam is most intense where the particle density of the other beam is changing most rapidly, at about one transverse beam sigma. The integrated signal over the bunch can be measured as the beams are steered through each other. An SLC beamstrahlung measurement is shown in Figure 15. The signal shape can have a single peak or two peaks, depending on the initial sizes of the two beams[46].

In practice, the art of spot size minimization presents a challenge for the SLC[47]. Information from the beam-beam deflections is an integral over both transverse beam distributions. Unraveling which beam parameter has the error requires a subtle deconvolution. Single beams can be imaged on wire scanners 20 cm from the IP but only at low currents. However, new effects enter the problem as the currents are increased. This inability to measure the size of a single beam at high currents slows the tuning procedure for making small spots. For example, the match of the beta function at the IP using beam-beam deflections is very hard if the mismatch is large. To complicate matters, non-linear dispersion effects have been observed on occasion in the positron beam in the final focus appearing as parabolic x-y profiles. The correction of this effect must be made not only in the final focus but also upstream in the arcs.

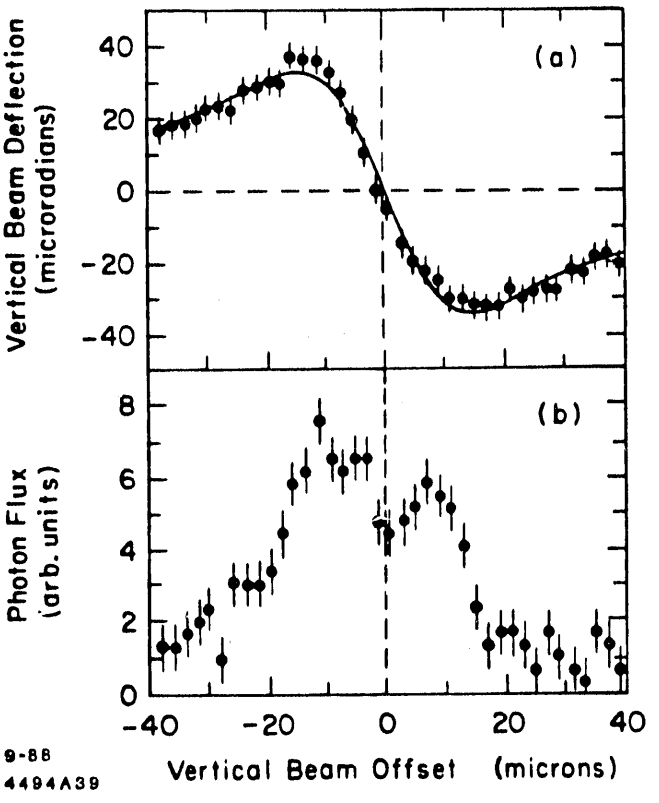

Figure 15 Observed beam-beam deflections at the interaction point in the upper plot. A beamstrahlung signal (radiated photons from the beam-beam interaction) is shown in the lower plot.

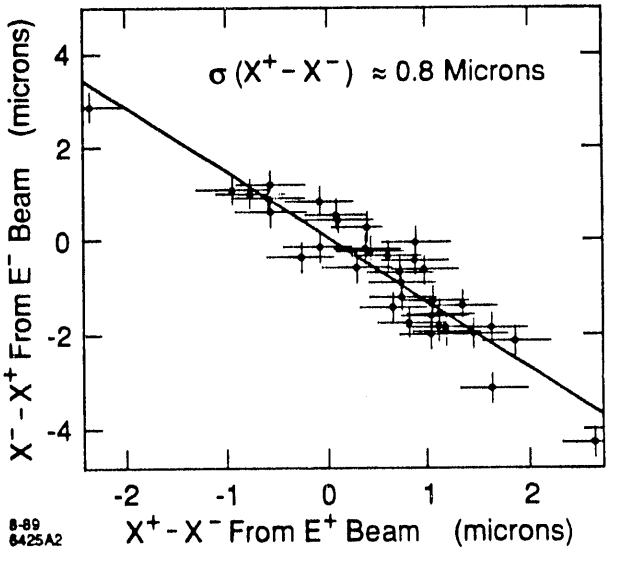

Figure 16 Measured relative beam position jitter at the interaction region determined from beam-beam deflections pulse-by-pulse. The correlation along the line indicates relative beam jitter and the line width is a measure of the instrumental error. $\sigma_{x,y} = 2.5$ μm.

9.0 Polarization

A polarized electron source with a bulk GaAs photocathode was tested in late 1991 with the goal of providing longitudinally polarized electrons at the IP[48]. All components of the gun system were commissioned and produced good results for its first two week run. A single bunch charge of 7 x 10^{10} e^- per pulse was achieved. Two polarized electron bunches with the appropriate timing were also produced. In the future, these two bunches will be handled exactly the same as unpolarized bunches downstream of the gun, with the exception of injection and extraction from the damping ring. The transport line from the linac to the damping ring is designed to have the proper energy and spin precession angle so that a superconducting solenoid (6.4 Tesla-meter) located in that line rotates the spin into the vertical direction for injection into the ring. The vertical spin remains polarized during the damping cycle if care is taken to avoid depolarizing resonances. On extraction, the bunches pass through two similar solenoids, one in the ring-to-linac transport line and the other in the early linac. These solenoids are used to align the spin in the precise orientation to make longitudinally polarized electrons at the IP after many precession cycles, both horizontally and vertically, in the SLC arcs.

During the tests of the polarized gun in the fall of 1991, an unexpected charge limit[49] relating to quantum efficiency was discovered, which reduces the charge obtainable in the second bunch. The physics of this limit is not yet understood.

10. SLC results

The luminosity of the SLC has grown steadily during commissioning. The increase in luminosity follows approximately an exponential curve with an e-folding time of about two months. The growth is highly correlated with accelerator physics studies and new hardware[50]. The integration of luminosity has likewise increased. The results of the 1991 run are shown in Figure 17.

The number of active components in the SLC, including power supplies, klystrons, kickers, vacuum pumps, computers, controls, and instrumentation, is nearly an order of magnitude larger than that of recently built circular electron colliders. Since a very large fraction of these components must be operational in order for the accelerator to function, the reliability of each component must be greater. Much effort is spent at SLAC to maintain reliable active components. The reliability of SLC operations[51] has increased to levels around 60%.

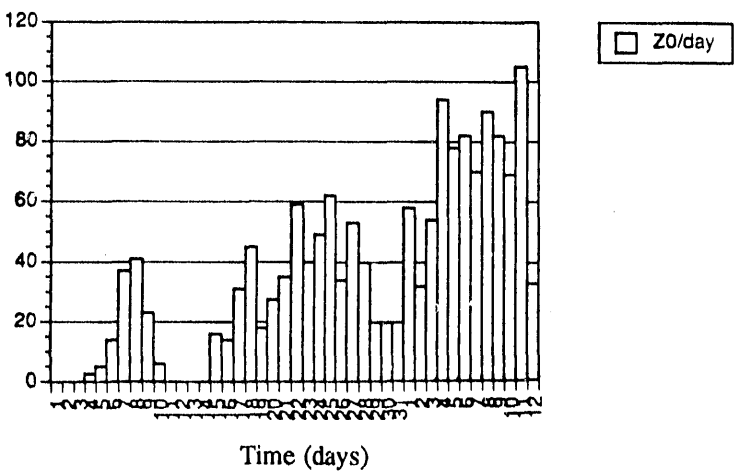

Figure 17 Integrated events per day delivered by the SLC to the SLD detector from July 1 through August 12, 1991. Over 100 Z^0 per day have been delivered.

11.0 Acknowledgments

Many people, too numerous to list here, from the Stanford Linear Accelerator Center and from around the world have contributed to the accelerator physics advances of the SLC.

12.0 References

1. R. Erickson, ed.,"SLC Design Handbook", Stanford (1984).
2. J. Seeman, *Annu. Rev. Nucl. Part. Sci.*, 41, p. 389-428 (1991).
3. M. Breidenbach, et al., "SLC Performance in 1991", SLAC Report Stanford (1990).
4. J. Clendenin, et al., *IEEE Trans. Nucl. Sci.* 28, p. 2452 (1981).
5. M. Ross, private communication.
6. A. Kulikov, et al., SLAC-PUB-5473, Stanford (1991).
7. T. Limberg and M. Ross, private communication.
8. J. Fox and P. Corredoura, SLC Experimental Report 253, Stanford (1991).
9. J. Seeman, et al., SLC Experiment Reports 244 and 248, Stanford (1991).
10. T. Limberg, et al., SLC-SLC-CN-387, Stanford (1991).
11. W. Spence, et al., SLAC-PUB-5276, Stanford (1991).
12. J. Sheppard, SLAC-CN-298, Stanford (1985).
13. P. Emma, et al., SLAC-PUB-5484, Stanford (1990).
14. C. Adolphsen, et al., SLAC-PUB-5584, Stanford (1991).
15. J. Seeman, SLC Experiment Report 250, Stanford (1991).
16. J. Seeman, et al., SLAC-PUB-5437, Stanford (1991).
17. K. Bane, SLAC-PUB-5177, Stanford (1990).
18. J. Seeman, *IEEE Trans. Nucl. Sci.*, 89CH2669-0, p. 1736 (1989).
19. J. Seeman, SLAC-PUB-5716, Stanford (1991) and *5th ICFA Advanced Beam Dynamics Workshop*, Corpus Christi, October (1991).
20. K. Bane and P. Wilson, *11th Int. Conf. on High Energy Accel.*, Birkhauser, p. 592 (1980).
21. V. Balakin, et al., *12th Int. Conf. on High Energy Accel.*, FNAL, p. 119 (1983).
22. J. Seeman, SLAC-PUB-4968, Stanford (1991)
23. J. Seeman and L. Merminga, *1990 Linear Accelerator Conf.*, Albuquerque, p. 387 (1990).
24. V. Balakin, *Proc. of 1st Intl. Workshop on Next-Generation Linear Collider*, Stanford: SLAC-Report-335, p. 56 (1988).
25. J. Seeman, SLC Experiment Report 221, Stanford (1991).
26. C. Adolphsen, et al., SLAC-PUB-4902, Stanford (1989).
27. T. Raubenheimer and R. Ruth, SLAC-PUB-5355, Stanford (1991).
28. J. Seeman, *Proc. 1990 Linear Accel. Conf.*, Los Alamos Natl. Lab., LA-12004-C, p. 390 (1990).
29. A. Chao, B. Richter, and C. Yao, *Nucl. Inst. and Meth.* 178, p. 1 (1980).
30. R. Stiening, SLAC-SLC-CN-161, Stanford (1982).
31. A. Chao, et al., see Ref. 29.
32. K. Bane, *IEEE Trans. Nucl. Sci.* NS-32, No. 5, p. 2389 (1985).
33. J. Seeman, et al., SLAC-PUB-5705, Stanford (1991).
34. J. Seeman, SLAC-PUB-5706, Stanford (1991).
35. J. Seeman, see Ref. 28.
36. T. Himel, et al., SLAC-PUB-5470, Stanford (1991).
37. J. Seeman, et al., SLC Experiment Report 249, Stanford (1991).
38. J. Seeman, SLC Experiment Report 252, Stanford (1991).
39. J. Seeman, SLAC-SLC-CN-330, Stanford (1986).
40. G. Fischer, et al., *IEEE Trans. Nucl. Sci.* NS-32-5, p. 3657 (1985).
41. T. Barklow, et al., *Part. Accel.* 30, p. 121 (1990).
42. N. Walker, et al., SLAC-PUB-5695, Stanford (1991) and *5th ICFA Advanced Beam Dynamics Workshop*, Corpus Christi, October (1991).
43. W. Spence, private communication.
44. P. Bambade, et al., SLAC-PUB-4776, Stanford (1989).
45. P. Bambade, et al., *Phys. Rev. Lett.* 62:2949 (1989).
46. G. Bonvicini, et al., *Phys. Rev. Lett.* 62:2381 (1989).
47. N. Toge, et al., SLAC-PUB-5553, Stanford (1991).
48. J. Clendenin, et al., SLAC-PUB-5368, Stanford (1991).
49. J. Clendenin, J. Frisch, A. Kulikov, D. Schultz, and M. Woods, private communication.
50. J. Seeman, SLAC-SLC-CN-377, Stanford (1991).
51. N. Phinney, SLC Experiment Report 254, Stanford (1991).

END

DATE
FILMED
2 12092

I